Correction of Drop Shape–Induced Errors on Rain Rates Derived from Radar-Measured Doppler Spectra at Vertical Incidence

DIRK KLUGMANN AND CAROLIN RICHTER

Meteorological Institute of the University of Hamburg, Hamburg, Germany

8 October 1993 and 5 May 1994

ABSTRACT

The shape of larger raindrops shows a deviation from spheres. This leads to a radar backscatter cross section different from the Rayleigh cross section. The drop shape–induced error for deducing rain rates is calculated. The resulting correction factor is applied to radar data measured during the CLEOPATRA field campaign in 1992. Depending on the drop size distribution, the correction led to reductions of the rain rate up to 10%. Furthermore, it is shown that the drop shape–induced error can be used as an indicator for drop size distribution.

1. Introduction

Vertically pointing Doppler radar is a powerful tool for precise rain-rate measurements. Furthermore, drop size distributions can be obtained that, for example, are necessary to study precipitation and wet deposition processes. In recent years, many techniques have been published to derive rain rates from Doppler radar spectra (Hauser and Amayenc 1981, 1983; Wakasugi et al. 1986, 1987; Gossard and Strauch 1990; Richter et al. 1992; and others) and to estimate corrections related to the shift of the Doppler spectra by vertical air motions and to the broadening of the spectra by turbulence. If the corrections are applied carefully, the method becomes so accurate that it is worthwhile to consider smaller errors that have been neglected in the past.

In this paper the error induced by the assumption of spherical drop shapes is examined in order to further increase the accuracy of rain rates measured by radar. Although the general expression for the radar cross section of oblate droplets is well known (Russchenberg 1992 or de Wolf et al. 1990), no correction of the error caused by using the Rayleigh scattering formula for perfect spheres has been applied until now. Furthermore, there is no report to the authors' knowledge about the actual size of this error for vertically pointing radar.

Since 1989 the L-band wind profiler of the University of Hamburg operating in FM-CW mode has been used for rain-rate measurements. For the CLEOPATRA (Cloud Experiment Oberpfaffenhofen and Transports) field campaign in summer 1992 (Meischner et al. 1993), the wind profiler was totally calibrated, and numerous datasets were acquired during rain events. Results derived from two selected datasets will be presented in this paper.

2. Derivation of rain rate from Rayleigh radar scattering

The radar cross section for spherical particles, which are small compared to the wavelength (Rayleigh scattering), is

$$\sigma_{\text{Rayleigh}} = \frac{\pi^5}{\lambda^4}\left|\frac{(\epsilon_r - 1)}{(\epsilon_r + 2)}\right|^2 a_0^6 \left(\frac{\pi a_0}{\lambda} \ll 1\right), \quad (1)$$

where a_0 denotes the particle diameter, λ the wavelength of the incident radiation, and ϵ_r the permittivity of the drop medium (for water, $\epsilon_r = 81.1$).

From radar measurements, the spectral radar reflectivity $Z(v)$ can be derived as a function of droplet fall velocity. The fall velocity is related to the equal volume diameter a_0 [$a_0 \approx (ab^2)^{1/3}$, where a and b denote the principal axes of the droplet] by the formula

$$v_*(a_0) = 9.65 \text{ m s}^{-1} - 10.3 \text{ m s}^{-1} \exp(-0.6a_0)$$
$$(1.09 \times 10^{-3} \leqslant a_0 \leqslant 6), \quad (2)$$

which was found by Atlas et al. (1973) and is based on empirical data of Gunn and Kinzer (1949). The diameter range of a_0 (mm) assumes that drops burst at a size of 6 mm (Pruppacher and Klett 1978). The effect of variation of air density with height is taken into account by a correction factor $(\rho_0/\rho)^{0.4}$ suggested by Foote and du Toit (1969),

$$v(a_0) = v_*(a_0)\left(\frac{\rho_0}{\rho}\right)^{0.4},$$

Corresponding author address: Dirk Klugmann, Meteorologisches Institut, Universität Hamburg, Bundesstraße 55, D-20146 Hamburg, Germany.

where ρ is the air density at the level of observation and ρ_0 is the air density at ground level. The spectral reflectivity $Z(v)$ at a determined range gate r can be found by

$$Z(v) = \frac{r^2}{c}\frac{\lambda^4}{\pi^5}\left|\frac{(\epsilon_r + 2)}{(\epsilon_r - 1)}\right|^2 P(v),$$

where $P(v)$ is the reflected spectral power received by the radar. The constant c contains the technical parameters of the radar and is very sensitive to the calibration of the radar. Since $Z(v)$ also satisfies the equation

$$Z(v) = N[a_0(v)]a_0^6(v)\frac{da_0}{dv},$$

the droplet spectra $N(a_0)$ (number of droplets per unit volume as a function of drop diameter a_0) can be deduced. Hence, the complete radar reflectivity spectrum of rain drops measured by radar at vertical incidence can be used to derive rain parameters (rain rate, liquid water content, drop size distribution) without assuming any drop size distribution (as, e.g., mentioned by Atlas et al. 1973). The rain rate R is defined by

$$R = \frac{\pi}{6}\int_0^\infty v(a_0)a_0^3 N(a_0)da_0. \qquad (3)$$

The influence of vertical wind is to shift the Doppler spectrum on the velocity axis, whereas the effect of turbulence is to broaden the spectrum. The error of the rain rate due to these effects can be calculated, and corrections can be applied if the magnitude of the vertical wind and/or turbulence is known.

3. The drop shape–induced error

With increasing size the drop shapes become increasingly oblate, and the ratio of b (the projected droplet width) to a (the projected droplet height) departs from unity. The volume of such spheroids can be expressed by the equal volume diameter a_0 (diameter of a sphere of the same volume). The diameter a_0 is related to a and b by the relation $a_0 \approx (ab^2)^{1/3}$ (Gunn and Kinzer 1949), and the inverse axis ratio $\beta = b/a$ is empirically defined by

$$\beta = 0.9 + 0.1a_0 \quad (a_0 > 1)$$

(Beard 1976), where a_0 is in millimeters. An example for $a_0 = 2.5$ mm from Pruppacher and Klett (1978) is shown in Fig. 1.

Due to the deviation of the drop shape from spherical, the radar cross section differs from the assumed Rayleigh cross section [Eq. (1)]. This influences the value of radar reflectivity that is related to the radar cross section σ by

$$Z = \sum_v a_0^6 = \frac{\sum_v \sigma}{(\lambda^4/\pi^5)\,|(\epsilon_r + 2)/(\epsilon_r - 1)|^2}.$$

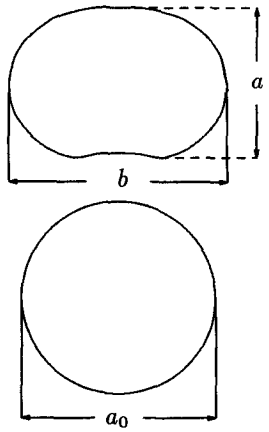

FIG. 1. Shape of an oblate waterdrop with axes a and b and spherical waterdrop with equivolumic diameter $a_0 = 2.5$ mm.

The canting effect of drops can be neglected, assuming that the canting angle is small (<3°) at altitudes above 100 m AGL (Brussard 1976). When the a axis is parallel to the drop fall direction, the radar-measured cross section is given by (Russchenberg 1992)

$$\sigma_{if} = \frac{\pi^5}{\lambda^4}\frac{a_0^6}{9}(\epsilon_r - 1)^2 q_{if}(a_0), \qquad (4)$$

where the $q_{if}(a_0)$ are defined by

$$q_{hh}(a_0) = [(\Lambda_3 - \Lambda_1)\cos^2\theta \sin^2\phi + \Lambda_1]^2$$

$$q_{vv}(a_0) = [(\Lambda_3 - \Lambda_1)\cos^2\theta \cos^2\phi + \Lambda_1]^2$$

$$q_{hv}(a_0) = \left[\frac{1}{2}\sin 2\phi \cos^2\theta(\Lambda_3 - \Lambda_1)\right]^2,$$

and Λ_1 and Λ_3 are factors representing different kinds of spheroids (de Wolf et al. 1990). The subscripts i and f denote polarization of the incoming and outgoing (scattered) electromagnetic waves; v and h indicate vertical and horizontal polarizations, respectively. The elevation angle of the radar is described by θ, and ϕ is the polarization angle of the radar. The latter is the angle between the horizontal polarization vector and the plane defined by the wave propagation vector and the a axis (short axis) of the spheroid droplet. When the radar antenna is at vertical incidence ($\theta = 90°$), the definition of ϕ becomes ambiguous, since the area illuminated by the electromagnetic wave is a circle and there is no cross polarization:

$$q_{hh}(a_0) = q_{vv}(a_0) = \Lambda_1^2$$

$$q_{hv}(a_0) = 0$$

$$\Lambda_1 = \frac{1}{[1 + \lambda_1(\epsilon_r - 1)]}.$$

For oblate spheroids, the depolarization factors λ_1 and λ_3 are (Russchenberg 1992)

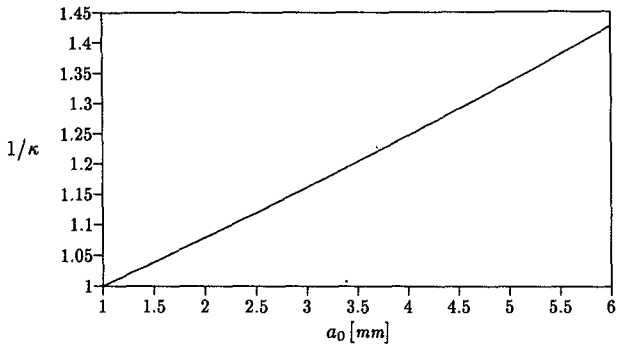

FIG. 2. Ratio $1/\kappa$ of radar cross section of spheroids to Rayleigh cross section as defined by Eq. (5).

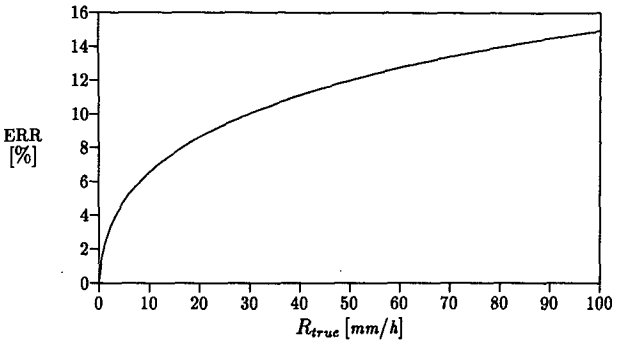

FIG. 3. Percentage relative error ERR as given by Eq. (7) versus rain rate R_{true} simulated from Marshall–Palmer distribution.

$$\lambda_1 = \frac{1 - \lambda_3}{2}$$

$$\lambda_3 = \frac{1 + f^2}{f^2}\left(1 - \frac{1}{f}\arctan f\right)$$

$$f^2 = \beta^2 - 1, \beta > 1.$$

The resulting ratio of the different radar cross sections [Eq. (1) vs Eq. (4)] as a function of the diameter a_0 is shown by Fig. 2.

Since the radar-measured drop size distributions are derived from the Rayleigh cross section σ_{Rayleigh}, the number $N(a_0)$ is overestimated by a factor of

$$\frac{1}{\kappa(a_0)} = \frac{\sigma_{if}(a_0)}{\sigma_{\text{Rayleigh}}(a_0)} = \frac{(\epsilon_r + 2)^2\, q_{if}(a_0)}{9}, \quad (5)$$

and the true number of droplets has to be calculated by the formula

$$N_{\text{true}}(a_0) = \kappa(a_0) N(a_0). \quad (6)$$

For increasing rain-rate intensities, the fraction of larger droplets contributing to an overestimation of drop number $N(a_0)$ is also growing. Consequently, the percentage relative error ERR, which is defined as

$$\text{ERR} = \frac{R - R_{\text{true}}}{R_{\text{true}}} \times 100\%, \quad (7)$$

depends on the rain rate R_{true}.

The true number $N_{\text{true}}(a_0)$ can be inserted into Eq. (3), and the integration is performed numerically to derive the corrected radar rain rate. To simulate Doppler radar spectra for various rain rates, $N_{\text{true}}(a_0)$ was calculated according to the Marshall–Palmer distribution (Marshall and Palmer 1948)

$$N_{\text{MP}}(a_0, R_{\text{true}}) = 8 \times 10^3\, e^{-\Lambda a_0} \quad (\Lambda = 4.1 R_{\text{true}}^{-0.21}),$$

where R is given in units of millimeters per hour and N_{MP} in units of per millimeter per cubic meter. This drop size distribution was inserted in Eq. (6) to find the distribution $N(a_0)$, given by an uncorrected radar measurement, and to derive the corresponding percentage relative error ERR. The results for rain rates up to $R_{\text{true}} = 100$ mm h^{-1} are shown in Fig. 3.

4. Application to radar-measured data

Time series of true rain rate R_{true} from radar-measured Doppler spectra $Z(v)$ at 200 m AGL (solid line) and the corresponding percentage error ERR induced by oblate drop shape (dotted line) are shown in Fig. 4. The first dataset was composed of 60-s averages taken during the CLEOPATRA field campaign 11 July 1992 in southern Germany using the 1.25-GHz FM-CW Doppler radar wind profiler of the University of Hamburg. The effects of vertical wind and turbulence have been neglected; also it should be noted that the standard deviation of the error due to vertical wind during this special rain event was less than or equal to 13% (Richter 1993). Assuming that the standard deviation of the turbulent velocity distribution is Gaussian and that $\sigma \sim 0.7$ m s^{-1} for rain, the error of the calculated rain rate is about 10% (Richter 1994).

For two selected Doppler spectra recorded at 1549 and 1606 MET (mid European time), respectively (in Fig. 4 marked by dashed vertical lines), the drop size

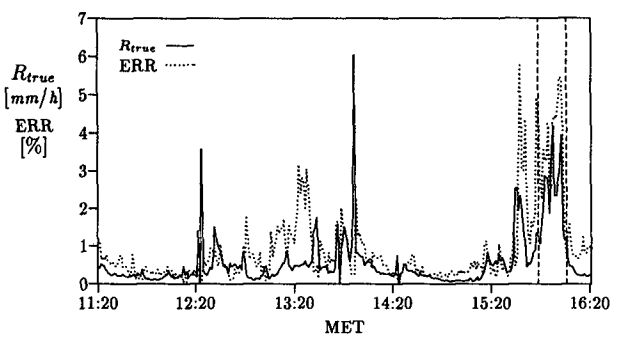

FIG. 4. Time series of radar-derived true rain rate R_{true} and corresponding drop shape–induced error ERR measured at CLEOPATRA field campaign 11 July 1992. The measuring height was 200 m and the averaging time was 60 s.

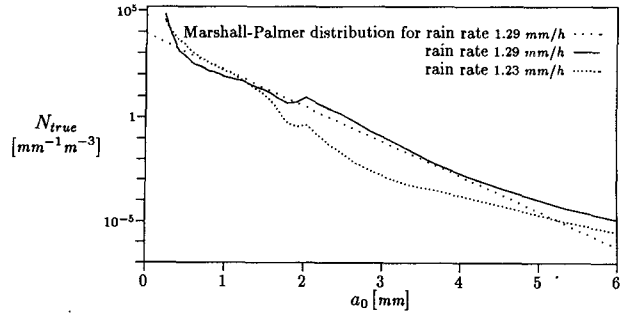

FIG. 5. Two selected drop size distributions from Fig. 4. The drop size distribution for R_{true} = 1.29 mm h^{-1} was measured at 1549 MET and the distribution for R_{true} = 1.23 mm h^{-1} at 1606 MET. As a comparison, the Marshall–Palmer distribution for R_{MP} = 1.29 mm h^{-1} is shown.

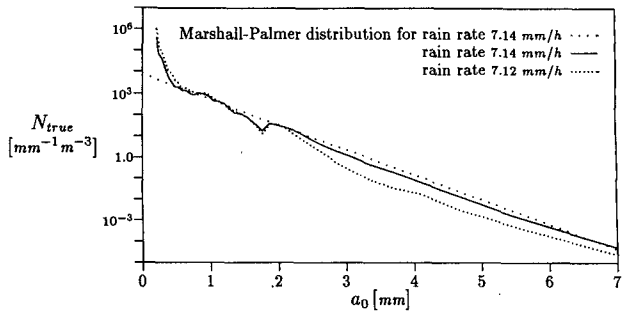

FIG. 7. Drop size distributions from Fig. 6. The drop size distribution for R_{true} = 7.14 mm h^{-1} was measured at 1957 MET and the distribution for R_{true} = 7.12 mm h^{-1} at 2000 MET.

distributions are shown in Fig. 5. The first spectrum (solid line) is recorded before a period of heavier rain, whereas the second one (dotted line) is recorded after this period. The number of larger drops (2–5 mm) for the first spectrum is 1–2 orders of magnitude greater than for the second one. In consequence, the drop shape–induced error for the first spectrum is higher (4.5%) than for the latter (0.8%). As a comparison, the Marshall–Palmer distribution for R_{MP} = 1.29 mm h^{-1} (widespread dotted line), which should lead (refer to Fig. 3) to a percentage relative error ERR $\approx$ 2.3, is also shown. The local minimum of the measured drop size spectra at $a_0 \approx 1.8$ mm is an artifact (velocity aliasing) caused by properties of the applied electronical filter. This also is the case for Fig. 7.

A second time series of rain rate R_{true} and percentage relative error ERR also sampled during CLEOPATRA is presented in Fig. 6. The data were taken on 22 July 1992 at 450 m AGL, with an averaging time of 10 s. Again, errors due to vertical wind and turbulence are neglected. In this case it wasn't possible to estimate the vertical wind, but other studies suggest an error of less than or equal to 20% (Richter 1994). Generally the percentage error ERR follows the rain rate R_{true} much better than during the 11 July case (Fig. 4). Nevertheless rainfall rates and the drop size–induced error ERR do not always track each other as illustrated by the period of heaviest rainfall around 2000 MET. The value of ERR decreases, although the rain rate R_{true} is still high.

Again two selected drop size distributions from times of similar rain rate are shown before (1957 MET) and after (2000 MET) a period of very intensitive rain (Fig. 7). In the range 3 mm $\leq a_0 \leq$ 6 mm, the drop size spectrum of 1957 MET (solid line) is at least half an order of magnitude higher than that of 2000 MET (dotted line). This consequently leads to percentage relative errors of ERR = 5.11 for the first spectrum and ERR = 3.35 for the second.

The contour plot of drop number versus equal volume diameter a_0 and time for the data of 22 July (Fig. 8) gives an overview of the development of drop size spectra for 1900–2040 MET. At 1920 MET and between 2000 and 2020 MET significant changes in drop size distribution can be observed that can be related to an increasing rain rate (compare with Fig. 6).

In particular, between 2000 and 2020 MET, the number density for drops smaller than 2.5 mm does

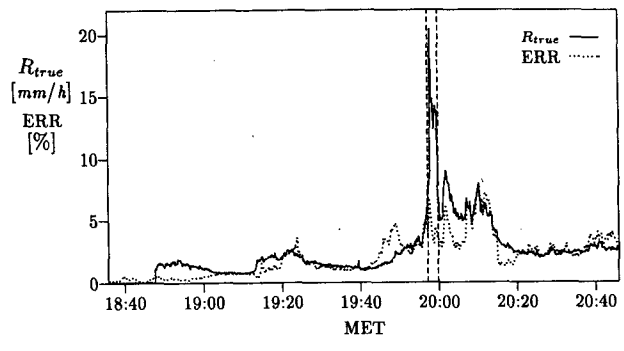

FIG. 6. Time series of radar-derived true rain rate R_{true} and corresponding drop shape–induced error ERR measured at CLEOPATRA field campaign 22 July 1992. The measuring height was 450 m and the averaging time was 10 s.

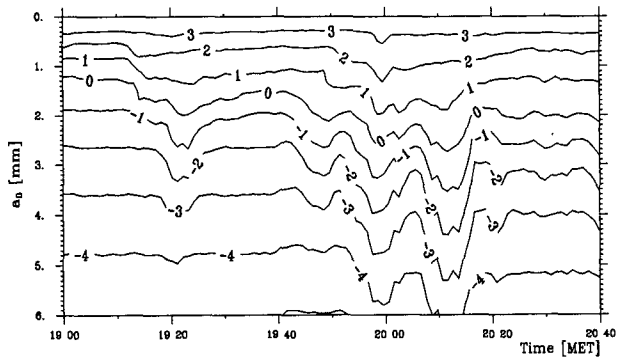

FIG. 8. Contour plot of drop number log$N(a_0)$ (mm^{-1} m^{-3}) versus equivolumic diameter a_0 and time. Data are corresponding to Fig. 6 but data have been averaged to 60 s.

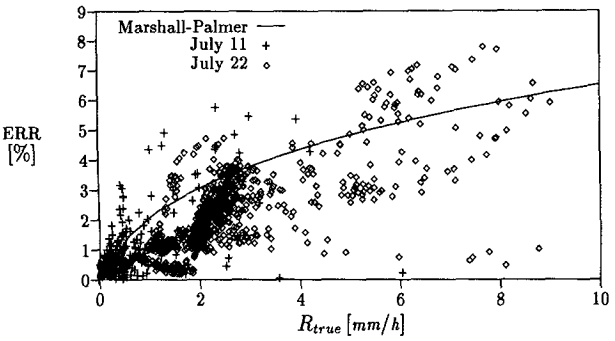

FIG. 9. Scatterplot of drop size–induced percentage relative error versus rain rate. The points correspond to measured rain events displayed in Figs. 4 and 6. The solid line shows the error of Marshall–Palmer distributed rain for comparison.

not change significantly (except for a short timed maximum in the first few minutes), while the number of larger drops is increased by at least one order of magnitude. This leads to a significant rise of the error ERR.

A scatterplot is presented in Fig. 9, which shows the error ERR versus the true rain rates using the data from Figs. 4 and 6. The function of drop size–induced error ERR caused by the Marshall–Palmer distributions for the given rain rates is superimposed.

It is obvious that the measured errors display a wide scatter compared to the values expected from the Marshall–Palmer distribution. For rain rates less than 4 mm h^{-1} most of the measured errors are lower than the one given by the Marshall–Palmer distribution. For higher rain rates, the theoretical data are a better representation of the empirical data. This is consistent with the drop size distributions presented in Figs. 5 and 7.

Another characteristic of the approximately 1000 data points presented in the scatterplot is the clustering effect. This suggests that the relation between error and rain rate is case dependent. Further studies of this behavior will be done with other CLEOPATRA data, as well as with existing measurements from other campaigns.

5. Conclusions

The analysis of the drop shape–induced errors shows that for heavy rain intensities, the value of the error can be up to ERR = 10%. This is in the same order of magnitude as other error sources (e.g., vertical wind, calibration) in radar-deduced rain rates and should not be neglected.

The measured error versus rain rate does not follow the function presumed by the Marshall–Palmer distribution. Furthermore the clustering of the examined data should be studied in more detail.

Acknowledgments. Taneil Uttal of NOAA/ERL/ETL provided useful comments and discussions to improve the readability and the style of this paper. This work was supported by the Deutsche Forschungsgemeinschaft (DFG) of the Federal Republic of Germany.

REFERENCES

Atlas, D., R. Srivastava, and R. Sekhon, 1973: Doppler radar characteristics of precipitation at vertical incidence. *Rev. Geophys. Space Phys.*, **11**, 1–35.

Beard, K., 1976: Terminal velocity and shape of cloud and precipitation drops aloft. *J. Atmos. Sci.*, **33**, 851–864.

Brussard, G., 1976: A meteorological model for rain-induced cross polarization. *IEEE Trans. Antennas Propag.*, **AP-24**, 5–11.

de Wolf, D., H. W. J. Russchenberg, and L. P. Ligthart, 1990: Effective permittivity of and scattering from wet snow and ice droplets at weather radar wavelengths. *IEEE Trans. Antennas Propag.*, **38**, 1317–1325.

Foote, G. B., and P. S. du Toit, 1969: Terminal velocity of raindrops aloft. *J. Appl. Meteor.*, **8**, 249–253.

Gossard, E., and R. Strauch, 1990: The retrieval of drop size distributions in water clouds from ground-based clear-air-sensing Doppler radar observations. *Meterolog. Rdsch.*, **42**(3–5), 165–173.

Gunn, R., and G. Kinzer, 1949: The terminal velocity of fall for water droplets in stagnant air. *J. Meteor.*, **6**, 243–248.

Hauser, D., and P. Amayenc, 1981: A new method for deducing hydrometeorsize distributions and vertical air motions from Doppler radar measurements at vertical incidence. *J. Appl. Meteor.*, **20**, 547–555.

——, and ——, 1983: Experimental size distributions of raindrops and vertical air motions deduced from vertically pointing Doppler radar data using a new method. *J. Climate Appl. Meteor.*, **22**, 407–418.

Marshall, J., and W. Palmer, 1948: The distribution of raindrops with size. *J. Meteor.*, **5**, 165–166.

Meischner, P., and Coauthors, 1993: The field project CLEOPATRA May–July 1992 in southern Germany. *Bull. Amer. Meteor. Soc.*, **74**, 401–412.

Pruppacher, H., and J. Klett, 1978: *Microphysics of Clouds and Precipitation.* Reidel, 714 pp.

Richter, C., 1993: A combined Doppler radar/RASS system as rain gauge. Preprints, *26th Int. Conf. on Radar Meteorology,* Norman, OK, Amer. Meteor. Soc., 646–647.

——, 1994: Niederschlagsmessung mit dem vertikal ausgerichteten FM-CW-Doppler radar-RASS-system—Validierung und anwendung (Measurements of precipitation with a FM-CW-Doppler radar-RASS system at vertical incidence—Validation and application). *Berichte aus dem Zentrum für Meeres-und Klimaforschung ZMK, Meteorologisches Institut, No. 12, Uni Hamburg,* Ph.D. thesis, 156 pp.

——, H. Jeske, and G. Peters, 1992: Das Doppler-radar als regenmeßgerät (Doppler radar as a tool for measuring rain). *Meteorolog. Zeitschrift,* **1**, 229–235.

Russchenberg, H. W. J., 1992: Ground-based remote sensing of precipitation using a multi-polarized FM-CW Doppler radar. Ph.D. Thesis, Delft University Press, 206 pp.

Wakasugi, K., and Coauthors, 1986: A direct method for deriving drop-size distribution and vertical air velocities from VHF Doppler radar spectra. *J. Atmos. Oceanic Technol.*, **3**, 623–629.

——, and Coauthors, 1987: Further discussion on deriving drop-size distribution and vertical air velocities directly from VHF Doppler radar spectra. *J. Atmos. Oceanic Technol.*, **4**, 170–179.